Chinese Chemical Letters 36 (2025) 110233

Contents lists available at ScienceDirect

Chinese Chemical Letters

journal homepage: www.elsevier.com/locate/cclet

Chlorination of benzyl group on the terminal unit of A_2-A_1-D-A_1-A_2 type nonfullerene acceptor for high-voltage organic solar cells

Jinge Zhu[a,b], Ailing Tang[b,*], Leyi Tang[a,b], Peiqing Cong[b], Chao Li[c,*], Qing Guo[d,*], Zongtao Wang[a,b], Xiaoru Xu[a,b], Jiang Wu[a,b], Erjun Zhou[b,*]

[a] School of Materials Science and Engineering, Zhengzhou University, Zhengzhou 450001, China
[b] National Center for Nanoscience and Technology, Beijing 100190, China
[c] Zhongyuan Critical Metals Laboratory, Zhengzhou University, Zhengzhou 450001, China
[d] Henan Institute of Advanced Technology, Zhengzhou University, Zhengzhou 450003, China

ARTICLE INFO

Article history:
Received 30 March 2024
Revised 8 July 2024
Accepted 10 July 2024
Available online 11 July 2024

Keywords:
High open-circuit voltage
Benzotriazole
Non-fullerene acceptor
Terminal engineering
Chlorination

ABSTRACT

Benzotriazole (BTA)-based A_2-A_1-D-A_1-A_2 type wide-bandgap (WBG) non-fullerene acceptors (NFAs) have shown promising potential in indoor photovoltaic, and in-depth investigation of their structure-property relationship is of great significance. Herein, we explored the chlorination effect of the side chain on the terminals. We introduced Cl atoms into the benzyl side chains in parent BTA5 to synthesize two NFAs, BTA5-Cl with mono-chlorinated benzyl groups and BTA5-2Cl containing bi-chlorinated benzyl groups. We chose D18-Cl with deep-energy levels and strong crystallinity to pair with these three acceptors, affording high photovoltage and photocurrent. With the stepwise chlorination, the open-circuit voltage (V_{OC}) values decrease from 1.28, 1.22, to 1.20 V, while the corresponding power conversion efficiencies (PCEs) improve from 5.07%, 9.15%, to 10.96%. Compared with BTA5-based OSCs, introducing Cl atoms downshifts the energy levels and slightly increases the non-radiative energy loss ($0.14 < 0.17 < 0.19$ eV), resulting in a sequential decrease in V_{OC}. However, more chlorine atom replacements produce more effective exciton dissociation, higher charge transfer, and balanced carrier mobility in the blend films, ultimately achieving better PCEs. This work indicates that chlorination of the benzyl group on the terminals can improve the device's performance, implying good application potential in indoor photovoltaics.

Organic solar cells (OSCs) have attracted widespread attention due to their advantages, such as low cost, light weight, solution processing, and large-area printing [1-6]. In the past few years, active layer materials have blossomed. A series of excellent polymer donors represented by PM6, PTQ10, and D18 have been developed, and multitudinous non-fullerene acceptors (NFAs) have sprung up [7-9]. The currently popular NFAs mainly apply A (acceptor)-D (donor)-A (acceptor) type and A-DA'D-A type skeleton structures [10]. The strong intramolecular charge transfer (ICT) endows these NFAs with broad absorption spectra, facilitating light-harvesting and thus significantly enhancing the short-circuit current (J_{SC}) [11]. So far, the power conversion efficiency (PCE) of single-junction and tandem OSCs based on A-DA'D-A type acceptors has exceeded 19% and 20%, respectively, under the standard AM 1.5G illumination [12-14]. Although the energy loss of the corresponding organic photovoltaic system has been reduced to around 0.5 eV, the open-circuit voltage (V_{OC}) is always below 1.0 V [15]. Once these OSCs work under indoor light conditions, V_{OC} will further decrease [16,17]. For example, PM6:Y6-O-based devices under 1-Sun condition can achieve a PCE of 16.53% with a V_{OC} of 0.94 V. Under 1650 lux 3000 K LED illumination, the PM6:Y6-O-based indoor device achieved a high PCE of 30.89%, but the V_{OC} is down to 0.84 V [18]. The ultra-low V_{OC} will increase the operating cost of industrialization. In addition, because the spectra of indoor light sources are located in the 400–750 nm range, such narrow bandgap acceptor materials could incur more losses due to spectral redundancy [10]. Hence, it is necessary to develop high-voltage wide-bandgap (WBG) photovoltaic materials that meet the requirements of indoor photovoltaics, which can fabricate high-efficiency indoor photovoltaics (IPVs) to power microelectronic devices in the Internet of Things (IoTs) [19,20].

Recently, several kinds of WBG NFAs with high lowest unoccupied molecular orbital (LUMO) energy levels have been developed through the precise design of electron-donating and electron-withdrawing units. For example, our group chose weak

* Corresponding authors.
E-mail addresses: tangal@nanoctr.cn (A. Tang), c.li@zzu.edu.cn (C. Li), qingg319@zzu.edu.cn (Q. Guo), zhouej@nanoctr.cn (E. Zhou).

https://doi.org/10.1016/j.cclet.2024.110233
1001-8417/

electron-withdrawing benzotriazole (BTA) as the A_1 unit and rhodanine derivatives as the A_2 unit to couple with indacenodithiophene (IDT) electron-donating unit and achieved some WBG A_2-A_1-D-A_1-A_2 type NFAs [21-23]. Due to the slightly weak intramolecular electron push-pull effect, these acceptors typically have wider bandgaps (~1.7–1.8 eV) and higher LUMO levels (LUMO > −3.8 eV). When blended with the donors having deep HOMO levels, the corresponding photovoltaic devices exhibited high V_{OC} exceeding 1.1 V. In 2019, we achieved a high V_{OC} of 1.24 V and a PCE of 10.5% by using the same A strategy to mix J52-Cl with BTA3 [24]. In 2023, BTA3–4F was synthesized by introducing F atoms into the side chains on the IDT unit. The photovoltaic device prepared with the terpolymer E18 and BTA3–4F obtained a V_{OC} of 1.3 V with a PCE of 10%, a breakthrough in this field [25]. These BTA-based wide-bandgap NFAs can be used as a third component to prepare ternary photovoltaic devices, effectively improving V_{OC} and assisting PCE breakthrough by over 19% [26]. Importantly, these BTA-based NFAs exhibited excellent performance in indoor photovoltaics. In 2021, PBDB-T:BTA3 achieved a PCE of over 25% under 1000 lux 2700 K LED illumination, and the system can still maintain a V_{OC} of about 1 V [27]. In the same year, Hou and his group designed a new wide-bandgap polymer PBQx-TCl to mix with BTA3, and the 1 cm^2 device obtained a 28.5% PCE with a V_{OC} of 1.10 V under indoor lighting [28]. In 2022, the tetrahydrofuran-processed ternary OSCs based on J52-Cl:BTA3:BTA1 afforded a PCE of 28.8% with a higher V_{OC} of 1.12 V under irradiation of a 1000 Lux light-emitting diode (LED) light [29]. Besides, D18:Cl-BTA5 devices can achieve a V_{OC} of 1 V and a PCE of 21% under indoor lighting conditions [20]. The large-area device (1 cm^2) that combined low-cost polymer PTQ10 with non-fused NFAs acceptor Cl-BTA33 can achieve a PCE of over 24% under indoor light exposure. Therefore, further exploring the structure-property relationship of these BTA-based molecules can help design new promising materials and develop high-efficiency IPVs.

As an effective molecular design strategy, halogenation has been widely applied in material design. The variation of positions and quantities of halogen atoms can lead to diverse photophysical properties and energy losses, leading to quite different device performance, for example, the classical NFAs, ITIC *vs.* IT-4F and Y5 *vs.* Y6 [30-32]. Our previous works have investigated the effect of halogenated on the BTA unit and central IDT unit in the BTA-based A_2-A_1-D-A_1-A_2 type NFAs [22]. The data indicated that introducing halogen atoms into the BTA unit had little influence on bandgap but lowered both the highest occupied molecular orbitals (HOMO) and LUMO energy levels, which can increase the charge transfer driving force and non-radiative recombination energy loss [33]. Introducing F atoms into the side chains on the central nucleus can increase molecular bandgap and change intermolecular interactions and stacking forms. Ultimately, both can improve device performance [34-36]. BTA5, with the benzyl group-substituted dicyanomethylene rhodanine as terminals, has shown improved device performance than BTA3 because the benzyl group could act on the intermolecular interaction patterns and facilitate the charge generation [37]. Further modifying the benzyl side chain and lucubrating their structure-performance relationship may achieve high photovoltaic performance.

Herein, with BTA5 as a benchmark, we study the impact of the chlorine atoms quantities in the terminal benzyl groups on device performance. Two BTA-based acceptor molecules, as shown in Fig. 1a, BTA5-Cl containing one chlorine atom in the benzyl groups and BTA5-2Cl bearing the two chlorine atoms in the benzyl groups, are synthesized. We chose D18-Cl (Fig. 1b) as the donor material to pair with the above three NFAs due to its deep HOMO level, high hole mobility, and strong crystallinity. D18-Cl:BTA5 has afforded the highest V_{OC} of 1.28 V with the smallest non-radiative recombination loss (ΔE_3) of 0.14 eV. ΔE_3 slightly increased from 0.14 eV to 0.17 and 0.19 eV, respectively, with the increase of chlorine atoms. As a result, the V_{OC} of D18-Cl:BTA5-Cl and D18-Cl:BTA5-2Cl are decreased to 1.22 V and 1.20 V, respectively. As the number of chlorine atoms in the terminals ascends, the molecular energy levels shift downward gradually, and the charge transfer driving force increases in order. At the same time, carrier mobilities become more balanced. Thus, the J_{SC} and fill factor (FF) increase sequentially. Finally, the D18-Cl:BTA5-2Cl device achieves the highest PCE of ~11%, with a V_{OC} of 1.20 V. These data indicate that the terminal side chains chlorination also plays an important role in the device's performance. Due to the matched absorption with the indoor sources, these high-V_{OC} OSCs have good potential for indoor OSC application.

The synthesis routes of the intermediate and small molecule acceptor BTA5-2Cl are provided in Fig. S1 (Supporting information). The ^{1}H NMR spectrum of the intermediate is depicted in Fig. S2 (Supporting information). BTA5 and BTA5-Cl were reported in our previous works [38]. The ^{1}H NMR, ^{13}C NMR, and mass spectra

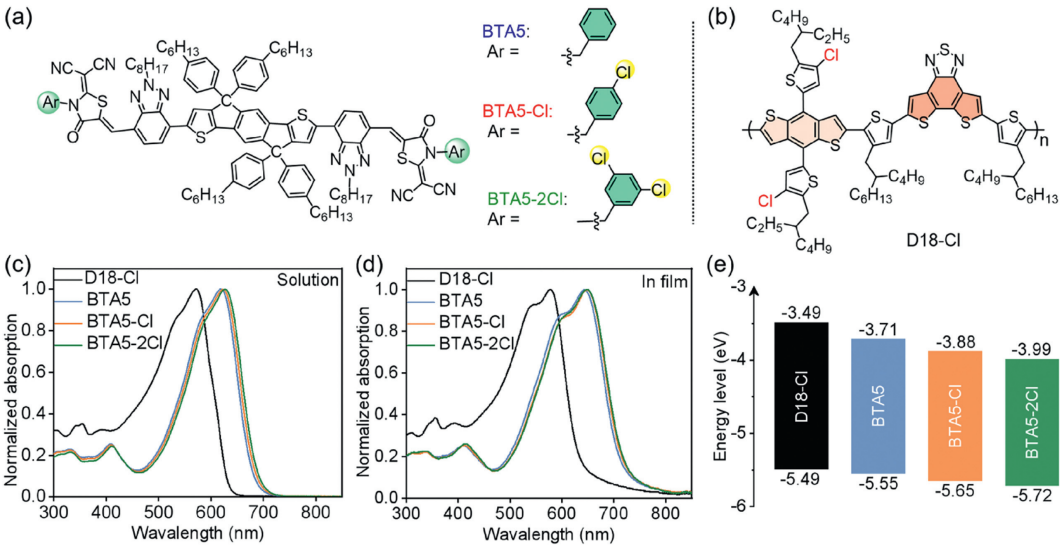

Fig. 1. Chemical structures of BTA5, BTA5-Cl and BTA5-2Cl (a) and the polymer D18-Cl (b). The absorption spectra of donor and three acceptors in chloroform solution (c) and neat films (d). (e) Energy levels diagram of D18-Cl, BTA5, BTA5-Cl and BTA5-2Cl.

of BTA5-2Cl are depicted in Figs. S3-S5 (Supporting information). Density functional theory (DFT) calculation based on the B3LYP/6–31G(d,p) basis set is performed on BTA5-2Cl. The calculated results in Fig. S6a (Supporting information) indicate that introducing different numbers of chlorine atoms on the end groups does not significantly alter the molecular conformation, and the three acceptor materials still exhibit a planar skeleton with negligible steric hindrance effects. Due to the increase in the number of halogen atoms, the electron-accepting ability of the corresponding acceptor is enhanced, and the energy levels of BTA5, BTA5-Cl, and BTA5-2Cl shift downwards, which could increase the energy offsets between the donors and acceptors and thus act on the V_{OC} and J_{SC}. In addition, we mapped the molecular surface electrostatic potential (ESP) distributions of the three acceptors (Fig. S6b in Supporting information). The overall ESP values on the molecular surfaces are almost positive for the three acceptors, and the overall average ESP values on the molecular surface increase with the addition of Cl atoms due to the electron-withdrawing property of the Cl atom. Gradually increasing ESP values could enhance intermolecular interactions with the polymer donor [39].

The ultraviolet-visible (UV–vis) absorption spectra of three systems in the $CHCl_3$ solution and thin film state are shown in Figs. 1c and d. The shape of the absorption spectrum has not undergone significant changes with the increase in the number of chlorine atoms in the side chain on terminals. As shown in Fig. 1c, the maximum absorption peaks of BTA5, BTA5-Cl, and BTA5-2Cl in the chloroform solution are 618, 622, and 627 nm, respectively, showing slight red-shifts as the increase of the Cl atoms. Compared with the solution absorption, the maximum absorption peaks of three acceptors in films significantly red-shift to 643, 648, and 651 nm, respectively, which indicates that all acceptors have strong intermolecular interactions in the thin films. With the increase of chlorine atoms, the absorption onsets are red-shifted. As a result, the optical bandgaps of BTA5, BTA5-Cl, and BTA5-2Cl are reduced from 1.84 eV to 1.77 and 1.73 eV, respectively. In addition, it is worth noting that BTA5-2Cl has the highest molar extinction coefficient of 1.82×10^5 L mol^{-1} cm^{-1}, while BTA5 and BTA5-Cl have similar molar absorption coefficients (1.35×10^5 L mol^{-1} cm^{-1} *vs.* 1.40×10^5 L mol^{-1} cm^{-1}). The higher extinction coefficient can enhance the light capture ability of the acceptor, thereby contributing to J_{SC}.

The effect of chlorination on the electrochemical property is investigated with cyclic voltammetry (CV). The CV curve of BTA5-2Cl is shown in Fig. S7 (Supporting information). As shown in Fig. 1e, the HOMO level of D18-Cl is −5.49 eV, and the LUMO level is −3.49 eV [40]. The $E_{HOMO/LUMO}$ energy levels are −5.55/−3.71, −5.65/−3.88, and −5.72/−3.99 eV for BTA5, BTA5-Cl [38], and BTA5-2Cl, respectively, implying that molecular energy levels decrease in order as Cl atoms increase. The variation trend of the molecular energy levels is consistent with the DFT calculation result. These data indicate that adding Cl atoms may provide a greater driving force for charge dissociation and help obtain higher J_{SC} but may sacrifice the V_{OC}.

To further estimate the influence of the Cl atoms on the photovoltaic performance, conventional devices are prepared with the structure of indium tin oxide (ITO)/poly(3,4-ethylenedioxythiophene):poly(styrene sulfonate) (PEDOT:PSS)/active layers/PFN-Br/Ag. The detailed device optimization process is shown in Tables S1-S3 (Supporting information), and the optimal device preparation conditions are provided in the supporting information. The optimal photovoltaic parameters of the three systems are listed in Table 1, and the corresponding current density-voltage (*J-V*) curves are presented in Fig. 2a. The devices based on D18-Cl:BTA5, D18-Cl:BTA5-Cl, and D18-Cl:BTA5-2Cl blends achieved a high V_{OC} of 1.28, 1.22, and 1.20 V, respectively. Increasing chlorine atoms on the terminal benzyl groups of the acceptors could gradually reduce the V_{OC}, which is attributed to the descending LUMO energy levels and increased energy loss. The J_{SC} values of the three devices rise as the number of Cl atoms increases, partly related to the increase of energy offsets between the HOMO levels of D18-Cl and these acceptors. D18-Cl:BTA5-2Cl device presents the highest J_{SC} value (12.89 mA/cm^2), higher than D18-Cl:BTA5 (7.38 mA/cm^2) and D18-Cl:BTA5-Cl (11.53 mA/cm^2). At the same time, the D18-Cl:BTA5-2Cl-based device achieves the highest FF of 0.71. D18-Cl:BTA5-Cl comes second (FF = 0.65), and D18-Cl:BTA5 is the worst (FF = 0.53). At last, the PCE of the D18-Cl:BTA5, D18-Cl:BTA5-Cl and D18-Cl:BTA5-2Cl blends are 5.07%, 9.15% and 10.96%, respectively. Fig. 2b shows the external quantum efficiency (EQE) curves of the optimized devices. The maximal EQE values of the three devices are 40%, 60%, and 67% for D18-Cl:BTA5, D18-Cl:BTA5-Cl, and D18-Cl:BTA-2Cl, respectively. The integrated current density (J_{cal}) values calculated from the EQE diagram are consistent with the current values calculated from the *J-V* curves.

Steady-state photoluminescence (PL) spectroscopy testing is used to investigate whether exciton dissociation had occurred in three mixed films. As shown in Fig. 2c, when selectively excited the acceptor with the excitation wavelength of 650 nm, the PL quenching rates of the three mixed films (D18-Cl:BTA5, D18-Cl:BTA5-Cl and D18-Cl:BTA5-2Cl) are calculated to be 62%, 86%, and 91%, respectively, indicating the gradually improved hole transfer efficiency. Increasing the number of Cl atoms on the terminals helps generate a more effective hole transfer, thereby facilitating the photocurrent generation.

We further apply the space-charge-charge-limited-current (SCLC) method to calculate the electron and hole mobility of three mixed films and study the effect of the number of chlorine atoms on the charge transport property [41]. The detailed device preparation process and calculation method are summarized in the supporting information. As shown in Figs. 2d and e, the electron mobilities (μ_e) of D18-Cl:BTA5, D18-Cl:BTA5-Cl, and D18-Cl:BTA5-2Cl are 1.79×10^{-4}, 2.94×10^{-4}, and 3.85×10^{-4} cm^2 V^{-1} s^{-1}, respectively, and the corresponding hole mobilities are 3.06×10^{-4}, 4.23×10^{-4}, and 4.98×10^{-4} cm^2 V^{-1} s^{-1}, respectively. The results show that with the increase of chlorine atoms in the acceptors, the electron and hole mobilities of the corresponding devices increase, and the electron mobilities increase more significantly. Thus, the ratio of μ_e/μ_h (0.58, 0.7, and 0.77) approaches closer and closer to 1 as the number of chlorine atoms increases. The more balanced carrier mobility in D18-Cl:BTA5-2Cl helps reduce charge recombination and facilitates higher J_{SC} and FF.

In order to understand the impact of the number of chlorine atoms on the charge recombination process, we studied the rela-

Table 1
Photovoltaic parameters of the optimized three OSCs.

Active layer	V_{OC} (V)	J_{SC} (mA/cm^2)	J_{cal} (mA/cm^2)[a]	FF (%)	PCE_{max}/PCE_{ave} (%)[b]
D18-Cl:BTA5	1.285	7.38	7.01	53.49	5.07 (4.86 ± 0.21)
D18-Cl:BTA5-Cl	1.223	11.53	10.95	64.98	9.15 (8.97 ± 0.18)
D18-Cl:BTA5-2Cl	1.202	12.89	12.24	70.77	10.96 (10.78 ± 0.18)

[a] The J_{cal} calculated from the EQE spectra.
[b] Average data from over 10 independent devices.

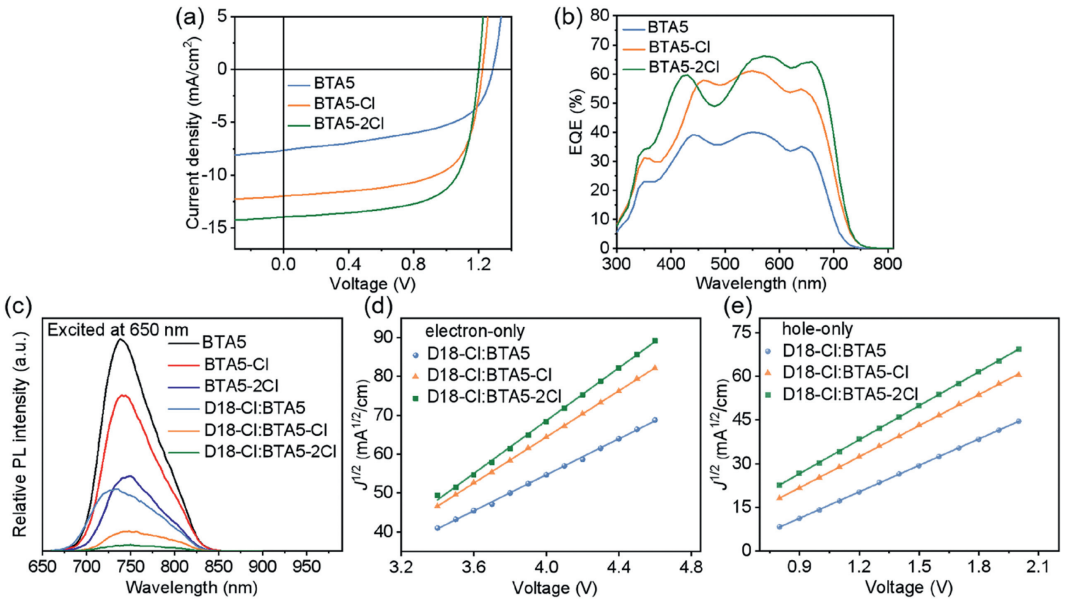

Fig. 2. *J-V* curves (a) and EQE spectra (b) of the OSCs based on D18-Cl:BTA5, D18-Cl:BTA5-Cl and D18-Cl:BTA5-2Cl. (c) The PL of neat films and blend films with excitation at 650 nm. $J^{1/2}$-*V* curves of electron-only (d) and hole-only (e) mobilities tested by the SCLC method.

tionship between J_{SC} or V_{OC} and the light intensity (P_{light}). The relationship between J_{SC} and P_{light} can be analyzed using the formula (Eq. 1):

$$J_{SC} \propto \left(P_{light}\right)^{\alpha} \tag{1}$$

When the value of α is closer to 1, bimolecular recombination is nearly inhibited [42]. As shown in Fig. S8 (Supporting information), the α values are 0.954, 0.966, and 0.967 for the devices based on D18-Cl:BTA5, D18-Cl:BTA5-Cl and D18-Cl:BTA5-2Cl, respectively. The D18-Cl:BTA5-2Cl device, with the highest α value, exhibits the lowest bimolecular recombination. The V_{OC} and light intensity relationship can be expressed with the formula (Eq. 2):

$$V_{OC} \propto \left(nkT/q\right)\ln\left(P_{light}\right) \tag{2}$$

The larger the n value, the more severe the monomolecular recombination or trap capture in the system, indicating a lower conversion efficiency of the device [43]. The *n* values of the three systems can be calculated as 1.45, 1.36, and 1.24, respectively. Compared with the other two systems, the monomolecular and trap-assisted recombination in D18:BTA5-2Cl is significantly suppressed, improving the J_{SC} and FF.

In order to investigate the effect of the number of chlorine atoms in the acceptor on energy loss, the FTPS-EQE spectra and EQE_{EL} curves were tested and depicted in Fig. S9 (Supporting information). The energy loss data of relevant devices are shown in Table S4 and Fig. S10 (Supporting information). The total energy loss can be divided into three parts (Eq. 3) [44]:

$$E_{loss} = \Delta E_1 + \Delta E_2 + \Delta E_3 \tag{3}$$

ΔE_1 is caused by radiative recombination loss above the bandgap, which is inevitable. It can be expressed using a formula (Eq. 4):

$$\Delta E_1 = E_g - qV_{OC}^{SQ} \tag{4}$$

where E_g is the bandgap of the D18-Cl:BTA5, D18-Cl:BTA5-Cl and D18-Cl:BTA5-2Cl, *q* is the element charge, and V_{OC}^{SQ} is the Shockley-Queisser (SQ) ultimate output voltage. The ΔE_1 of the related devices are 0.288, 0.285, and 0.285 eV. ΔE_2 is the radiative recombination below the bandgap, mainly caused by the absorption of the CT state. ΔE_2 can be calculated using the formula (Eq. 5):

$$\Delta E_2 = q\left(V_{OC}^{SQ} - V_{OC}^{rad}\right) \tag{5}$$

where V_{OC}^{rad} is the limited V_{OC} under only radiation recombination conditions. ΔE_2 of the D18-Cl:BTA5, D18-Cl:BTA5-Cl, and D18-Cl:BTA5-2Cl are 0.093, 0.082 and 0.083 eV, respectively. ΔE_2 is also related to energy disorder, which can be reflected with Urbach energy (E_U). As shown in Fig. 6a, according to the formula (Eq. 6) [45]:

$$\alpha(E) = \alpha_0 \exp\left[\left(E - E_g\right)/E_U\right] \tag{6}$$

The E_U values for BTA5-, BTA5-Cl-, and BTA5-2Cl-based devices are 37.2, 36.7, and 36.8 meV, respectively. The fluctuation of E_U values is consistent with the change of ΔE_2, indicating that introducing chlorine atoms into the terminals can slightly reduce energy disorder. ΔE_3 is the non-radiative energy loss, which can be calculated from the EQE_{EL} spectrum, according to the following formula (Eq. 7):

$$\Delta E_3 = q\left(V_{OC}^{rad} - V_{OC}\right) = -kT\ln\left(EQE_{EL}\right) \tag{7}$$

From Fig. S10a, the EQE_{EL} values for BTA5-, BTA5-Cl-, and BTA5-2Cl-based devices are 4.59×10^{-3}, 1.52×10^{-3}, and 6.99×10^{-4}, respectively. The corresponding ΔE_3 values are 0.139, 0.168, and 0.188 eV, respectively. $\Delta E_3 = 0.139$ eV, one of the lowest values in OSCs, is roughly the same as those of inorganic or perovskite solar cells [46-50]. Introducing chlorine atoms into the terminals can slightly reduce the luminescence efficiency, increasing ΔE_3 [51]. In summary, introducing Cl atoms could gradually increase energy loss from 0.520 eV to 0.535 and 0.556 eV. Hence, BTA5-2Cl with dichlorination attains the lowest V_{OC} of 1.20 V, followed by BTA5-Cl with mono-chlorination ($V_{OC} = 1.22$ V), and BTA5 without Cl atoms exhibits the highest V_{OC} of 1.28 V.

Contact angle testing is commonly used to study the miscibility between donor polymers and small molecule acceptors. The contact angles of D18-Cl, BTA5, BTA5-Cl, and BTA5-2Cl pure films were tested using water and diiodomethane, as shown in Fig. S11 (Supporting information). The detailed data are listed in Table S5 (Supporting information). The test results were analyzed using the Flory-Huggins theory, according to the formula (Eq. 8):

$$\chi = \mathrm{K}\left(\sqrt{\gamma_D} - \sqrt{\gamma_A}\right)^2 \tag{8}$$

where χ is Flory-Huggins interaction, K is the constant, and γ is the surface tension of the relevant material [52]. The calculated χ

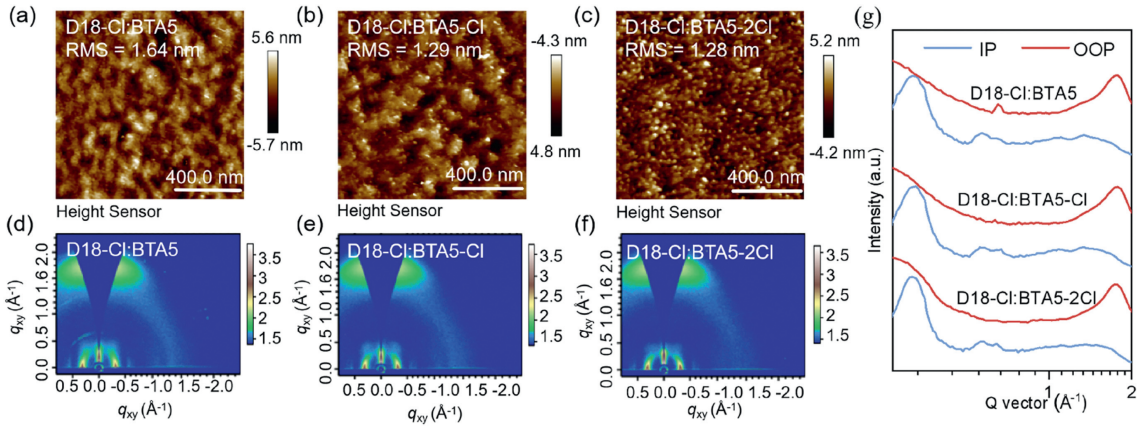

Fig. 3. Atomic force microscopy height images of D18-Cl:BTA5 (a), D18-Cl:BTA5-Cl (b) and D18-Cl:BTA5-2Cl (c). 2D GIWAXS patterns of D18-Cl:BTA5 (d), D18-Cl:BTA5-Cl (e), D18-Cl:BTA5–2Cl (f) and the corresponding 1D profiles (g).

values of the three devices are 0.69 K for D18-Cl:BTA5, 0.56 K for D18-Cl:BTA5-Cl, and 0.59 K for D18-Cl:BTA5-2Cl, respectively. The D18-Cl:BTA5-based device shows the largest χ values among the three devices, indicating that the miscibility of the device is the worst, which may form the large phase separation. The χ value decreases with the introduction of chlorine atoms, indicating the miscibility is improved, which is beneficial for charge transport and exciton dissociation, achieving higher FF and better PCE.

Atomic force microscopy (AFM) is used to study the surface morphology of the blend film. As shown in Figs. 3a-c, the root-mean-square (RMS) roughness of D18-Cl:BTA5, D18-Cl:BTA5-Cl, and D18-Cl:BTA5-2Cl are 1.64, 1.29, and 1.28 nm, respectively. Compared with the D18-Cl:BTA5 blend film, with the introduction of chlorine atoms, the active layer obtained a smoother surface, which is conducive to forming more effective charge extraction. These data are consistent with the data of the contact angle testing. To further investigate the influence of the number of chlorine atoms on molecular stacking and crystallinity, we conducted two-dimensional grazing-incident wide-angle X-ray scattering (2D GIWAXS) testing on three blend films. As shown in Figs. 3d-g, three blend films mainly exhibit an obvious (100) diffraction peak in the in-plane (IP) direction and a (010) diffraction peak in the out-of-plane direction, implying that all of the three films preferred the face-on orientation, which is conducive to charge transport. The detailed data is presented in Table S6 (Supporting information). BTA5, BTA5-Cl, and BTA5-2Cl exhibit similar π-π stacking distances of 3.57, 3.58, and 3.57 Å, respectively. The crystallite coherence lengths (CCL) of the (010) peak for BTA5, BTA5-Cl, and BTA5-2Cl are 20.86, 22.04, and 25.84 Å, respectively. Meanwhile, the corresponding CCLs of the (100) peak are 96.70, 104.11, and 115.42 Å in the IP direction. These data indicate that as the number of chlorine atoms increases, the crystallinity of the mixed film gradually increases, which is beneficial to charge transport, obtaining higher carrier mobilities and current values.

In summary, we introduced different numbers of chlorine atoms on the terminal benzene rings in BTA5 and obtained two NFAs, BTA5-Cl and BTA5-2Cl. D18-Cl, with deeper HOMO energy levels and strong crystallinity, was chosen as the polymer donor to pair with these acceptors and investigate the effect of the chlorine atom's quantities on the photovoltaic performance. Due to the low energy offsets and low non-radiative energy loss below 0.20 eV, these devices attain a high V_{OC} above 1.20 V. As the number of chlorine atoms increases, V_{OC} gradually decreases from 1.28 V to 1.22 V and 1.20 V, with the non-radiative energy loss increasing from 0.14 eV to 0.17 and 0.19 eV. BTA5-2Cl-based OSCs with the most Cl atoms achieve a PCE of nearly 11% due to more effective exciton dissociation and charge transfer capabilities, as well as more balanced carrier mobility. Our research results indicate that increasing the number of halogen atoms in the acceptor is beneficial for achieving better performance while maintaining a high voltage. Despite the non-conjugated nature of the substituents, chlorination remains effective in modulating the molecular energy levels. These results could provide important guiding principles for future molecular design.

Declaration of competing interest

The authors declare that they have no known competing financial interests or personal relationships that could have appeared to influence the work reported in this paper.

CRediT authorship contribution statement

Jinge Zhu: Writing – original draft, Investigation, Data curation. **Ailing Tang:** Writing – review & editing, Supervision, Project administration, Funding acquisition. **Leyi Tang:** Methodology, Data curation. **Peiqing Cong:** Methodology, Investigation, Data curation. **Chao Li:** Methodology, Investigation. **Qing Guo:** Supervision, Data curation. **Zongtao Wang:** Methodology, Investigation, Data curation. **Xiaoru Xu:** Methodology, Investigation. **Jiang Wu:** Methodology, Data curation. **Erjun Zhou:** Writing – review & editing, Supervision, Project administration, Investigation, Funding acquisition.

Acknowledgment

The authors thank the support from the National Natural Science Foundation of China (Nos. 52373176, 52073067).

Supplementary materials

Supplementary material associated with this article can be found, in the online version, at doi:10.1016/j.cclet.2024.110233.

References

[1] Y. Cui, H.F. Yao, J.Q. Zhang, et al., Adv. Mater. 32 (2020) 1908205.
[2] S. Dong, K.X. Zhang, B.M. Xie, et al., Adv. Energy Mater. 9 (2018) 1802832.
[3] G.U. Kim, J.H. Park, S. Lee, et al., J. Mater. Chem. A 10 (2022) 9408–9418.
[4] C.Q. Li, X. Zhang, N.G. Yu, et al., Adv. Funct. Mater. 32 (2022) 2108861.
[5] D.L. Liu, B. Yang, B. Jang, et al., Energy Environ. Sci. 10 (2017) 546–551.
[6] L. Wang, T.T. Wang, J. Oh, et al., Chem. Eng. J. 442 (2022) 136068.
[7] J. Yuan, Y.Q. Zhang, L.Y. Zhou, et al., Joule 3 (2019) 1140–1151.
[8] Q.S. Liu, Y.F. Jiang, K. Jin, et al., Sci. Bull. 65 (2020) 272–275.
[9] C.K. Sun, F. Pan, H.J. Bin, et al., Nat. Commun. 9 (2018) 743.
[10] A.L. Tang, P.Q. Cong, T.T. Dai, Z.T. Wang, E.J. Zhou, Adv. Mater. 35 (2023) 2300175.
[11] S.S. Li, L. Ye, W.C. Zhao, et al., J. Am. Chem. Soc. 140 (2018) 7159–7167.

[12] K. Chong, X.P. Xu, H.F. Meng, et al., Adv. Mater. 34 (2022) 2109516.
[13] L. Zhu, M. Zhang, J.Q. Xu, et al., Nat. Mater. 21 (2022) 656–663.
[14] R. Zeng, L. Zhu, M. Zhang, et al., Nat. Commun. 14 (2023) 4148.
[15] X.J. Li, F.S. Pan, C.K. Sun, et al., Nat. Commun. 10 (2019) 519.
[16] W.X. Wang, Y. Cui, T.B. Zhang, et al., Joule 7 (2023) 1067–1079.
[17] L. Xie, W. Song, J.F. Ge, et al., Nano Energy 82 (2021) 105770.
[18] X.B. Zhou, H.B. Wu, U. Bothra, et al., Mater. Horiz. 10 (2023) 566–575.
[19] F.J. Bai, J.Q. Zhang, A.P. Zeng, et al., Joule 5 (2021) 1231–1245.
[20] Z.T. Wang, A.L. Tang, H.L. Wang, et al., Chem. Eng. J. 451 (2023) 139080.
[21] B. Xiao, A.L. Tang, J. Yang, Z.X. Wei, E.J. Zhou, ACS Macro Lett. 6 (2017) 410–414.
[22] B. Xiao, A.L. Tang, J.Q. Zhang, et al., Adv. Energy Mater. 7 (2017) 1602269.
[23] A.L. Tang, B. Xiao, Y.M. Wang, et al., Adv. Funct. Mater. 28 (2018) 1704507.
[24] A. Tang, W. Song, B. Xiao, et al., Chem. Mater. 31 (2019) 3941–3947.
[25] T.T. Dai, A.L. Tang, Z.H. He, et al., Energy Environ. Sci. 16 (2023) 2199–2211.
[26] Y. Cui, Y. Xu, H.F. Yao, et al., Adv. Mater. 33 (2021) 2102420.
[27] Y. Yang, Z.H. Chen, T.Q. Wang, et al., Org. Electron. 98 (2021) 106289.
[28] Y. Xu, Y. Cui, H.F. Yao, et al., Adv. Mater. 33 (2021) 2101090.
[29] Q. Wu, Y. Yu, X.X. Xia, et al., Joule 6 (2022) 2138–2151.
[30] Q.P. Fan, W.Y. Su, Y. Wang, et al., Sci. China Chem. 61 (2018) 531–537.
[31] J.M. Cao, L.F. Yi, L.M. Ding, J. Semicond. 43 (2022) 030202.
[32] Y.X. Li, J.D. Lin, X.Z. Che, et al., J. Am. Chem. Soc. 139 (2017) 17114–17119.
[33] X. Liu, Y.X. Li, K. Ding, S. Forrest, Phys. Rev. Appl. 11 (2019) 024060.
[34] H. Zhang, H.F. Yao, J.X. Hou, et al., Adv. Mater. 30 (2018) 1800613.
[35] J.F. Huang, S.S. Li, J.Z. Qin, et al., ACS Appl. Mater. Interfaces 13 (2021) 45806–45814.
[36] Y.X. Tang, H.X. Feng, Y.Y. Liang, et al., ACS Appl. Polym. Mater. 5 (2021) 2298–2306.
[37] X.C. Wang, A.L. Tang, J. Yang, et al., Sci. China Chem. 63 (2020) 1666–1674.
[38] K.Y. Zuo, T.T. Dai, Q. Guo, et al., ACS Appl. Energy Mater. 5 (2022) 14271–14279.
[39] H.F. Yao, D.P. Qian, H. Zhang, et al., Chin. J. Chem. 36 (2018) 491–494.
[40] X.G. Li, Z.T. Wang, A.L. Tang, et al., Macromol. Rapid Commun. 44 (2023) 2300019.
[41] C. Zhu, J. Yuan, F.F. Cai, et al., Energy Environ. Sci. 13 (2020) 2459–2466.
[42] S.R. Cowan, A. Roy, A.J. Heeger, Phys. Rev. B 82 (2010) 245207.
[43] Y.F. Wang, J. Li, T.F. Li, et al., Small 15 (2019) 1903977.
[44] Z. Chen, X. Chen, Z.Y. Jia, et al., Joule 5 (2021) 1832–1844.
[45] F. Urbach, Phys. Rev. 92 (1953) 1324-1324.
[46] S. Liu, J. Yuan, W.Y. Deng, et al., Nat. Photonics 14 (2020) 300–305.
[47] Y.G. Cui, P.P. Zhu, H.W. Hu, et al., Angew. Chem. Int. Ed. 62 (2023) e202304931.
[48] P.Y. Zhang, Z.Y. Zhang, H. Sun, et al., Chin. Chem. Lett. 35 (2024) 108802.
[49] J.K. Zhang, B. Yu, Y.P. Sun, H.Z. Yu, Adv. Energy Mater. 13 (2023) 2300382.
[50] Z.P. Yu, X. Li, C.L. He, et al., Chin. Chem. Lett. 31 (2020) 1991–1996.
[51] N. An, Y.H. Cai, H.B. Wu, et al., Adv. Mater. 32 (2020) 2002122.
[52] H.J. Li, S.Q. Liu, X.T. Wu, et al., Energy Environ. Sci. 15 (2022) 2130–2138.